Journal of Chromatography, 465 (1989) 39–57
Elsevier Science Publishers B.V., Amsterdam — Printed in The Netherlands

CHROMSYMP. 1539

PACKING TECHNOLOGY, COLUMN BED STRUCTURE AND CHROMATOGRAPHIC PERFORMANCE OF 1–2-μm NON-POROUS SILICAS IN HIGH-PERFORMANCE LIQUID CHROMATOGRAPHY

H. GIESCHE*[a], K. K. UNGER, U. ESSER, B. ERAY and U. TRÜDINGER
Institut für Anorganische und Analytische Chemie, Johannes Gutenberg-Universität, D-6500 Mainz (F.R.G.)
and
J. N. KINKEL
Chemicals and Reagents Division, E. Merck, D-6100 Darmstadt (F.R.G.)

SUMMARY

This work is aimed at further elucidating the aggregation behaviour of micron- and submicron-size non-porous silicas and the column performance of 1–2-μm C_{18} silicas in reversed-phase high-performance liquid chromatography of low-molecular-weight compounds. It is demonstrated that highly ordered, dense, porous aggregates of such silica beads were obtained by gravity settling and centrifugation. The slurry techniques applied at constant flow-rate and a pressure up to 50 MPa provided less-ordered aggregates, but generated an acceptable performance of columns when 1–2-μm C_{18} silica beads were employed. To operate columns of 53 mm × 4.6 mm I.D., the maximum flow-rate needs to be *ca.* 2.5 ml/min at an inlet pressure of 50 MPa. To keep extra-column effects to a minimum, the injection volume should be about 0.6 μl, the volume of the detector cell about 0.3 μl and the time constant of the detector < 50 ms. Such columns enable fast separations of mixtures of low-molecular-weight substances in less than 30 s.

INTRODUCTION

The slurry, axial- and radial-compression techniques have been widely accepted as standard packing procedures in analytical and preparative high-performance liquid chromatography (HPLC)[1,2]. Each technique is applied in a number of variations, depending on the type of packing and column configuration. For instance, the slurry technique is carried out both with low- and high-viscosity solvent mixtures, at constant pressure or at constant flow-rate, upwards or downwards.

The main goal of a packing procedure is to achieve a homogeneous, dense and stable column bed, which generates the expected chromatographic performance and

[a] Present address: c/o Professor E. Matijević, Department of Chemistry, Clarkson University, Potsdam, NY, 13676, U.S.A.

0021-9673/89/$03.50

provides an adequately long column lifetime. It has been demonstrated that columns packed with spherical particles exhibit better chromatographic properties than those with irregularly shaped particles of the same size and size distribution[3]. Yet, it is still a matter of debate to which extent the width and the shape of the particle size distribution and the porosity of the packing affects the column quality[4,5].

In order to examine the bed structure and performance of analytical HPLC columns, we used as model packings non-porous 1–2-μm silicas, which were recently developed in our laboratory[6]. The material consists of uniform and monodisperse non-porous spheres. The mean particle diameter could be adjusted between 0.5 and 3.5 μm with a standard deviation of the mean, based on the number average, of less than $\pm 5\%$. The material is composed of amorphous silica of a bulk density of 2.20–2.25 g/ml. It possesses a hydroxylated surface. Thus, the traditional chemical modification procedures can be applied to make any type of bonded phase. The lack of internal surface area and porosity makes the beads less susceptible to compression during packing than porous particles. The small particle size of about 1 μm generates a high back pressure and limits the column length to about 50 mm. On account of the extremely small particles, the columns are able to perform highly rapid and efficient separations, provided the HPLC equipment is properly designed. The low surface area of about 1–3 m^2/ml, compared to *ca.* 100 m^2/ml for porous silicas, decreases the mass loadability for low-molecular-weight substances by a factor of 50, as the mass loadability is proportional to the surface area of the packing.

This study falls into two parts. In the first part, we attempted to assess the column bed structure of compacted non-porous silica beads by applying various established techniques in powder agglomeration and in HPLC. The data permit to compare the packed aggregates in terms of the interstitial pore volume, the mean pore diameter and the packing structure, and to judge the performance of the various aggregation techniques. The packing structure is directly related to the column performance, in particular to the column plate height (via the A-term of the Knox equation) and to the column pressure drop (via the column resistance factor Φ)[43].

Thus, in the second part the peak height–linear velocity dependencies measured on slurry-packed 1–2-μm columns and the pressure drop are compared with the theoretically predicted values. In addition, the chromatographic performance data obtained are discussed under the aspects of the practical limitations where short columns packed with these particles are used for fast separations.

Results on 1–2-μm spherical porous silicas have also been reported by Dewaele and Verzele[7], Unger *et al.*[8] and Danielson and Kirkland[9,10].

EXPERIMENTAL

Materials

The silica spheres were prepared by hydrolyis of tetraethoxysilane in ethanol–water–ammonia mixtures in two ways[6].

Procedure A

Silica spheres of a projected area diameter, $d_{p_n}^{p.a.}$, of <0.5 μm were synthesized following the Stöber process[11].

Procedure B

Spheres of $d_{p_n}^{p,a}$ in the range 0.2–3.5 μm were prepared by subjecting the silica suspensions made according to procedure A to a slow, controlled size-growth process, applying a dilute tetraethoxysilane solution[6]. By careful control of the experimental conditions a layer-by-layer growth of the native particles occurred without a second nucleation.

The suspensions were allowed to settle, and the particles were obtained by removing the supernatant solution. In separate experiments, an *in situ* silanization of the external surface of the silica spheres was performed by substituting the dilute tetraethoxysilane solution in the controlled size-growth process by a solution of ethyltriethoxysilane and *n*-octyltriethoxysilane[6]. The products are abbreviated as C_2 modified and C_8 modified. The native silica beads "as made" were subjected to the following treatments: (1) calcination at 823 K over a period of 48 h; (2) rehydroxylation by refluxing the beads in an aqueous suspension or in 1 *N* nitric acid at 373 K for 4 days; (3) silanization by a reaction of the dried silica beads with N,N-dimethylaminodimethyl-*n*-octylsilane according to a procedure described elsewhere[12]. The batches prepared are listed in Table II.

Tetraethoxysilane, obtained from Wacker (Burghausen, F.R.G.), was distilled over calcium oxide (b.p. = 441 K, n_D^{20} = 1.383). Water was quartz-distilled and deionized. Ammonia solution (25%, w/w), ethanol and acetonitrile were of analytical grade (Merck, Darmstadt, F.R.G.). Test substances were benzene, naphthalene, biphenyl, fluorene, anthracene, pyrene and chrysene (analytical grade, Merck).

METHODS

Aggregation techniques

Gravity settling and centrifugation. For gravity settling, either the actual silica suspension was used or the beads were isolated by freeze-drying and then suspended in deionized water or aqueous solution of pH 2.6, 5.3 or 10.9 at a concentration of about 1% (w/w). The suspensions were allowed to settle under vibration-free conditions. After settling was completed, the excess of solvent was carefully decanted. Drying was carried out sequentially in air, in a dessiccator over silica gel, at a vacuum of about 10 mbar at room temperature (24 h), and at 373 K (24 h).

As settling by gravity was extremely slow for batch B241/I of d_p = 89.6 nm, aggregation was performed by centrifugation. A centrifuge was applied with a rotor diameter of 15 cm at 680 (75 *g*) and 3000 (1450 *g*) rpm. After settling, the cake was carefully removed and dried under the previously described conditions.

Slurry technique. A stainless-steel HPLC column, 53 mm × 4.6 mm I.D. (Bischoff, Leonberg, F.R.G.), fitted at the lower end with metal frits and filter paper No. 827 (Schleicher & Schüll, Dassel, F.R.G.), was connected with its upper open end to a 100-ml autoclave. A 1% (w/w) suspension of the silica beads was made in ethanol–water (50:50, v/v) by ultrasonic treatment and poured into the autoclave with the column attached. After closing the autoclave, the suspension was pumped through the column at a constant flow-rate, raising the pressure to 50 (in the first experiment) or 100 (in the second) MPa. After filling, the pressure was slowly reduced. The column content was pressed out and dried as described for the gravity settling and centrifugation experiments.

Isostatic compression (dry bag). A tube made of poly(vinyl chloride) was filled with silica beads. It was then closed at both ends with rubber stoppers and placed in a high-pressure autoclave (Nova Suisse, Effretikon, Switzerland). The autoclave was filled with deionized water. After closing the autoclave, the pressure was raised stepwise. Four experiments were run with final pressures of 1.28, 8.0, 50 and 313 MPa, which were maintained over a period of 12 h. Then the pressure was released step-wise to atmospheric pressure over several hours, and the compacted spheres carefully removed after cutting the plastic tube.

Transmission electron microscopy (TEM) and scanning electron microscopy (SEM)

TEM was employed to assess the particle size distribution of the silica beads, and SEM served as a means of analyzing the packing structure of porous aggregates. TEM micrographs were obtained on a Philips (Kassel, F.R.G.) Model EM 300 electron microscope. The acceleration voltage of the electron beam was 80 kV. Magnification was $\times 1000$ to $\times 52\,000$. SEM micrographs were obtained on a Philips Model PSEM 500 electron microscope. The electron beam was focussed to 8–64 nm. For each sample, several micrographs were taken at a series of angles.

The micrographs were analyzed by an image analyzer (Videoplan; Kontron, Munich, F.R.G.). The mean particle diameter of the silica spheres calculated was the projected area diameter, based on the number-average $d_{p,n}^{p,a.}$ at 50% of the cumulative distribution curve. The precision in the particle size determination was less than $\pm 1\%$. The error of the calculated x,y,z coordinates of the beads was less than $\pm 5\%$.

Sorption measurements

Nitrogen sorption isotherms at 77 K were determined gravimetrically, using a microbalance (Model 4102 or 4433; Sartorius, Göttingen, F.R.G.). Samples were degassed until the sample mass remained constant (473 K, 10 h, final vacuum 10^{-4} Pa). Nitrogen was of 99.999% purity (Linde, Düsseldorf, F.R.G.). The saturation vapour pressure of nitrogen was measured close to the sample, employing a specially constructed device[13]. The pressure was recorded with a piezo-resistive pressure transducer (Model 4043A1; Kistler, Ostfildern, F.R.G.). From nitrogen sorption data the specific surface area according to the BET equation, a_s (BET) was calculated, using the molecular cross-sectional area of nitrogen, a_m (N_2) = 0.162 nm^2 (ref. 14).

Sorption isotherms of helium and xenon (purity 99.999%; Messer, Griesheim, F.R.G.) were performed on the dried and calcined silica beads at 298 K, using a magnetic suspension balance (Sartorius).

Mercury porosimetry

The porosimeter was constructed in our laboratory, as described in refs. 13 and 15.

The sample was weighed into the penetrometer, degassed and then filled with freshly distilled mercury. The volume of intruded mercury, v_p^{MP}, was measured as a function of increasing pressure. The pressure was recorded when equilibrium was achieved. The v_p^{MP} value was corrected by the compression of mercury and the penetrometer device[15]. After intrusion, the retraction branch was measured by releasing the pressure in steps. For some measurements, the intrusion was repeated after refraction.

The following parameters were calculated:

v_p^{MP} = the specific pore volume corresponding to the intruded volume of mercury at p_{max}.
PSD = the pore size distribution, calculated from the Washburn equation with a surface tension of mercury of 480 mN/m and a contact angle of mercury of 140° at 298 K (ref. 14).
pd_{50}^{MP} = the mean pore diameter, corresponding to the 50% value of the cumulative distribution.

Apparent helium, mercury and water densities

The apparent density of helium, d_{app} (He), was determined on a helium pycnometer (Model 930; Beckman, Munich, F.R.G.). The apparent mercury and water densities, d_{app} (Hg) and d_{app} (H_2O) were measured at 298 K, using a pycnometer of 0.8 ml volume[8]. The reproducibility of the density measurements was ±0.15%. The total specific pore volume was calculated by

$$v_p \text{ (total)} = \frac{1}{d_{app} \text{ (Hg)} - d_{app} \text{ (H}_2\text{O)}} \quad (1)$$

(or d_{app} (He) instead of d_{app} (H_2O))

Column packing procedures

For chromatographic tests, two batches of silicas were employed with $d_p^{p.a.} = 1.5$ and 2.1 μm. The silica beads were modified with monochlorodimethyl-*n*-octylsilane according to a procedure described elsewhere[12]. Suspensions of the *n*-octyldecyl-bonded beads were made in tetrachloromethane–paraffin (50:50, v/v) mixtures by ultrasonic treatment. The concentration of C_{18}-bonded silica was 5% (w/w). The silica was packed into columns of 33 mm × 8 mm and 53 mm × 4.6 mm (Bischoff) at a constant flow-rate and a maximum pressure of 50 MPa. The end-fittings were filter papers No. 827 (Schleicher & Schüll) supported by metal frits No. 22800812 (Bischoff).

Chromatographic measurements

The HPLC equipment consisted of a Model 2200 pump (Bischoff), a Model 7413 injection system (Rheodyne, Cotati, CA, U.S.A.) with a 0.5-μl sample loop, a variable-wavelength UV detector from Shimadzu (Düsseldorf, F.R.G.) with a detector cell volume of 0.6 μl and a time constant of 50 ms. The separation was repeated at 150 ms and 1.5 s. A Model C-R3A integrator from Shimadzu was used.

Thiourea was employed as unretained compound (t_m marker) to calculate the capacity factor of the test substances and the linear velocity, u.

The plate height, H, of the test substances was measured by means of the equation

$$H = \frac{L}{16} \left(\frac{w_t}{t_R}\right)^2 \quad (2)$$

where L is the column length, t_R the retention time and w_t the peak width in time units at 13.5% of the peak height.

RESULTS AND DISCUSSION

Characterization of the silica beads

The silica beads were synthesized by hydrolytic polycondensation of tetraethoxysilane in a two-step procedure[6]. The first step followed the procedure developed by Stöber *et al.*[11], yielding a suspension of colloidal silica particles up to about 0.5 μm of mean particle diameter. In a consecutive reaction, the particles were subjected to a slow, controlled size-growth process by means of hydrolysis of a dilute tetraethoxysilane solution, avoiding nucleation. In this way, particles up to a mean diameter of 3.5 μm were synthesized and isolated from the supernatant by sedimentation. The procedure developed has several attractive features, in particular, when the material is intended to be used in HPLC. The size of the beads covers a range that is still usable, with regard to column back pressure, in columns operated under normal HPLC conditions. No sizing is needed, as is essential in the manufacture of microparticulate porous silicas. The procedure described has been scaled up to batches of several kilograms. The size distribution is extremely narrow, i.e. the standard deviation of the mean particle diameter is smaller than ±5%. Fig. 1 shows the probability plot of the cumulative size distribution curve of two batches. The median projected diameter, based on a number average, and the standard deviation of the median were: batch B241/III (431 ± 9.2) nm, batch B241/IV (1002 ± 21.2) nm. The shape factor, f, being the axial ratio of an ellipsoid with the same inertial moment, varied between 0.95 and 0.98.

Characteristics of aggregated 1-μm and submicron silica beads

Colloidal silica particles of submicron size have a tendency to aggregate, due to

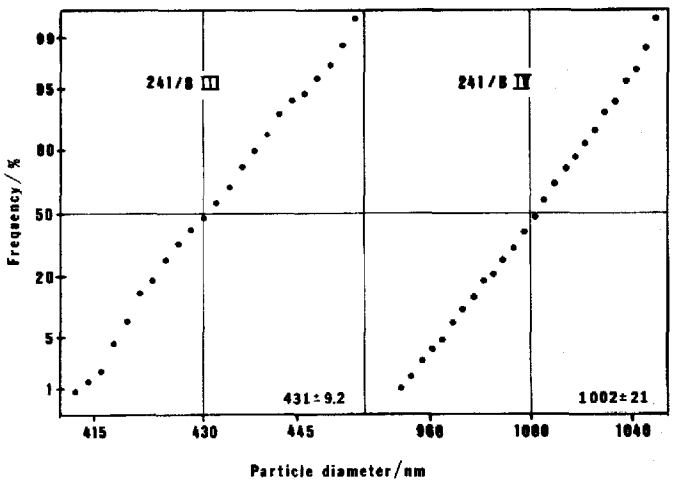

Fig. 1. Probability plot of the cumulative size distribution curve of sample B241/III (d_p = 431 ± 9.2 nm) and B241/IV (d_p = 1002 ± 21.2 nm).

their high surface area-to-volume ratio. Aggregation of colloidal silica is usually accomplished by gelling, coagulation, flocculation and coacervation, in which the assembled particles form a less-ordered three-dimensional network[16]. Aggregation must be clearly distinguished from agglomeration. By definition, in aggregates, the particles are loosely coherent, while in agglomerates they are rigidly joined together[17]. Correspondingly, the processes applied for aggregation and agglomeration differ. Agglomeration processes can be divided into hard- and soft-based, depending upon whether excess pressure is applied or not[18,19]. Soft processes comprise bead granulation and spray-drying, while agglomeration under pressure is carried out by isostatic compression, extrusion, and other modes employing the dry or wet powder, a paste or a suspension.

Aggregation procedures applied in this study were gravity settling and centrifugation. To prepare dense aggregates, the traditional HPLC slurry technique was employed, with pressures between 50 and 100 MPa, and the dry-bag isostatic compression technique, with pressures between 1 and 300 MPa. On account of the small size of the colloidal particles and of the relatively high pressures, particle bridging might occur in the latter. In addition to 1-μm particles, smaller beads were chosen down to a d_p of 90 nm. The silica beads were used in their native state, calcined, and *n*-alkyl-silanized.

Model structures originating from packed, uniform spheres have been examined by Heesch and Laves[20], Manegold[21], Kadaner *et al.*[22], Meissner *et al.*[23], Ridgeway and Tarbuck[24], and Karnaukhov[25]. Characteristic parameters describing these close-packed spheres were the type of structure, the contact number per sphere, the void volume or porosity, the diameter of a sphere inscribed in the cavities, and the diameter of the circle inscribed in the throats connecting the cavities[26]. In order to estimate these parameters on aggregates of uniform spheres the following methods were applied: nitrogen sorption, mercury porosimetry (MP), SEM, and optical diffraction. In a previous study at this laboratory, the pore structure of synthetic opal of a particle size of $d_p = 220$ nm and of an aggregate of colloidal silica particles made by the Stöber process of $d_p = 310$ nm were analyzed[26]. The synthetic opal displayed the closest packing of spheres with a contact number of 12 and a porosity of 26.3%.

Porosity and mean pore diameter of the aggregates. To study the effect of the soft and hard aggregation techniques on the porosity and pore diameter, a batch of 1-μm silica beads was employed and subjected to heat treatment at 473 K. The properties of the product were: d_p, 954 ± 22 nm, $f = 0.95$, $d_{app}(He) = 2.04$ g/ml.

The porosities of bodies of packed uniform spheres have been reported as: hexagonal and cubic close-packed, 25.95%; body-centered tetragonal, 30.18%; primitive hexagonal, 39.54%; primitive cubic, 47.64%; and tetrahedral, 66.01%[27]. The pore diameter, expressed as the diameter of the inscribed circle in the throats, pd_{th}, calculated according to Karnaukhov[28,29] for an aggregate of regularly packed uniform spheres, is

$$pd_{th} = 2.8\ v_p/a_{s(ext)} \cdot 10^3/\text{nm} \tag{3}$$

where v_p is the specific pore volume in ml/g and $a_{s(ext)}$ the external surface area in m^2/g, given by

$$a_{s(ext)} = 6/d_p d_{app}(He) \quad (4)$$

Using $d_{app}(He) = 2.04$ g/ml and $d_p = 954$ nm, $a_{s(ext)}$ is calculated to be 3.1 m^2/g. Thus, the closest-packed structure of spheres with porosity, $P = 26\%$ and $v_p = 0.172$ ml/g would result in a pore diameter of $pd_{th} = 147$ nm $= 0.147$ μm.

Table I lists the values of v_p, P, and the mean pore diameter pd_{50}^{MD}, assessed by mercury porosimetry, of aggregates obtained by gravity settling, centrifugation and the two pressure compaction methods. When aqueous suspensions of the silica beads are used, the surface charge of the particles comes into play. The point of zero charge of suspended silica particles lies in the range between pH 1 and 2, although higher values have been reported[30], measured by the electrokinetic mobility of silicas in suspensions of different pH. With increasing pH, the negative charge of the particles increases, the particles repel each other, and the suspension becomes more stable. As a result, notably higher packing densities and corresponding lower porosities were achieved with aggregates settled by gravity and by centrifugation at pH 10.9 than at pH 2.6. In spite of the favourable conditions, the porosities found were slightly higher than those for the densest array of packed spheres (26%). The decrease in porosity with rising pH of the suspension is accompanied by a diminution in the pore diameter. The mean pore diameters, measured by MP, were in the order of those calculated by eqn. 4, using $a_{s(ext)} = 3.1$ m^2/g.

The porosities of aggregates obtained by the slurry technique reflect the same tendency with regard to the pH of the suspension as was observed for aggregates made by settling and centrifuging. As expected, the dry-bag isostatic compression technique led to a densification of aggregates with rising pressure. At a pressure of 313 MPa, some of the particles were seen to show cracks and fissures. This phenomenon did not occur with silanized silica beads when ethyltriethoxysilane was used as a reagent under otherwise constant conditions. In general, the porosities of aggregates made of the silanized beads were slightly lower than those for beads made of parent silica (see values in Table I in parentheses). This might be a result of the weaker particle-to-particle interactions of the silanized beads, which cause a higher lateral mobility under the compression forces.

Batches of silica beads of $d_p = 89.6$, 199, 431 and 1002 nm in the native, thermally treated, rehydroxylated and silanized state were chosen to examine the effect of the nature of the surface on the settling behaviour and on the properties of the aggregates (see Table II). Rehydroxylation of the calcined beads slightly increased the mean pore diameter due to the hydrothermal treatment of porous aggregates (*cf.* batches B241/I and B241/II). The consecutive silanization with *n*-octyldimethylaminosilane narrowed the pore diameter by nearly the thickness of a fully extended *n*-octyl layer (about 2 nm) and also decreased the porosity. Silica beads, modified with ethyltriethoxysilane *in situ* and aggregated, gave generally higher packing densities and lower porosities than those made from beads modified *in situ* with *n*-octyltriethoxysilane. It is probable that the long-chain alkyl groups hinder a close attachment of the spheres during settling in aqueous suspensions. Burning off the carbon layer by calcination at 823 K slightly increased the packing density. The aggregated C_2 product, subjected to calcination at 823 K, showed the same porosity or even smaller porosity than the native calcined material without any modification, whereas the aggregated C_8 product could not be densified by calcination to such an extent.

TABLE I

RESULTS OF AGGREGATION EXPERIMENTS WITH *CA.* 1-μm NATIVE AND SILANIZED MONODISPERSE SILICA PARTICLES

v_p^{MP} = Specific pore volume from the mercury intrusion curve at p_{max}; P = porosity; pd_{50}^{MP} = mean pore diameter at 50% of cumulative distribution curve from mercury porosimetry. The batch of $d_p = 954 \pm 20$ nm was prepared according to the same procedure as batch B241/IV (see Table II). Values in parentheses refer to the silanized silica particles.

Mode of aggregation	d_p *of starting silica (nm)*	*Variable*		v_p^{MP} *(ml/g)*	*P (%)*	pd_{50}^{MP} *(nm)*
		pH of suspension	*Pressure (MPa)*			
Centrifugation	954 ± 20	2.6		0.456	48.3	337
		5.3		0.372	43.2	284
		7.0		0.351	41.8	293
		10.9		0.305	38.4	275
Gravity settling	954 ± 20	2.6		0.428	46.7	367
		10.9		0.33	40.3	279
Slurry technique (100 MPa)	954 ± 20	2.6		0.437	47.2	371
		5.3		0.380	43.7	334
		7.0		0.370	43.1	307
		10.9		0.353	41.9	290
Isostatic compression	954 ± 20		1.28	0.481	49.6	489
			8.0	0.422 (0.354)	46.3 (42.0)	466 (355)
			50	0.409 (0.376)	45.5 (43.5)	449 (364)
			313	0.285 (0.273)	38.3 (35.8)	344 (282)

Structure of aggregates. Two methods were chosen to elucidate the structure of aggregates: SEM and MP. SEM has the advantage of providing direct images of the aggregates. Disadvantages are that small domains of the exterior structure are always seen and, hence, sufficiently many photographs are required to get a representative image of the whole material. Also stereo-SEM should be applied to avoid false interpretations of the structure.

In MP mercury as a non-wetting liquid is intruded into the void space of the aggregates by gradually raising the pressure. Frevel and Kressley[31] have computed theoretical porosimetry curves for aggregates of uniform microspheres on the basis of the interconnected-void model. The characteristic feature is an abrupt threshold mercury penetration. It is assumed that this phenomenon is attributed to the sudden penetration throughout the interconnected voids, followed by a gradual filling of toroidal voids around the point of contact between two particles. Mayer and Stowe[32,33] have improved the model, introducing the breakthrough pressure as a decisive parameter, which was defined in terms of the porosity of the aggregate and the contact angle of mercury. Their model structure was an assembly of spheres, grouped in hexagonal close-packed layers, with vertically stacked layers above and below.

It is common to normalize the pressure by means of the equation

$$p^* = p\, d_p / 2\gamma_{L,v} \tag{5}$$

where p^* is the normalized pressure, p the equilibrium pressure, d_p the diameter of the

TABLE II

RESULTS OF AGGREGATION EXPERIMENTS WITH NON-POROUS SILICAS OF VARIOUS PARTICLE SIZES, NON-SURFACE-MODIFIED AND SILANIZED, NON-CALCINED AND CALCINED AT 823 K

Batch No.	d_p *(nm)*	*Procedure*	*Mode of aggregation*	*Aggregates of*	v_p^{MP} *(ml/g)*	*P (%)*	pd_{50}^{MP} *(nm)*
B241/I	89.6 ± 6.6	A	Centrifugation	Native beads	0.249	33.1	20.6
				In situ C_2-modified beads	0.220	30.4	17.1
				In situ C_8-modified beads	0.273	35.2	25.9
				Native beads calcined at 823 K and rehydroxylated	0.218	32.8	21.1
				Native beads calcined at 823 K and rehydroxylated, C_8-modified	0.190	29.8	19.1
B241/II	199 ± 6.8	B (batch B241/I)	Gravity settling	*In situ* C_2-modified beads	0.201	31.1	30.7
				In situ C_2-modified beads calcined at 823 K	0.195	30.4	31.8
				In situ C_8-modified beads	0.244	35.3	40.2
				In situ C_8-modified beads calcined at 823 K	0.231	34.1	42.9
				Native beads calcined at 823 K	0.208	31.8	38.8
				Native beads calcined at 823 K, rehydroxylated	0.203	31.3	40.0
				Native beads calcined at 823 K, rehydroxylated, C_8-modified	0.191	29.2	37.5
B241/III	431 ± 9.2	B (batch B241/II)	Gravity settling	*In situ* C_2-modified beads	0.183	26.7	69.9
				In situ C_2-modified beads calcined at 823 K	0.179	28.6	86.0
				In situ C_8-modified beads	0.207	29.2	77.7
				In situ C_8-modified beads calcined at 823 K	0.173	30.3	91.2
				Native beads calcined at 823 K	0.173	27.9	141
B241/IV	1002 ± 21.2	B (batch B241/III)	Gravity settling	*In situ* C_2-modified beads	0.231	31.5	259
				Native beads calcined at 823 K	0.203	31.3	307

primary particles of the aggregates and $\gamma_{L,v}$ the surface tension of mercury. Values of p^* for the breakthrough pressure reported in the literature, are 4.06 (ref. 31), 4.0 (ref. 34) and 3.18–4.41 (ref. 35).

The mercury intrusion curves were measured for a number of aggregates, made by gravity settling, and plotted as the intruded volume of mercury against the normalized breakthrough pressure. Usually the breakthrough into the pore system occurred at p^* values of 8 to 10. In the case of some less dense packings, the breakthrough started at more or less lower values of about 4.5 to 5.0. Occasionally, a two-step intrusion was observed. According to Mayer and Stowe[32,33], the first value corresponds to a close-packed structure of spheres, assuming a contact angle of mercury of 130–140°C. The first value fits a structure with a packing angle σ = 70–80°, where the layers are laterally displaced and show defects.

The high value of the breakthrough pressure of 9–10 has never been reported before in the literature. It appears, that it is associated with the highly regular and dense structure of aggregates. Iczkowski[36] has shown, that the breakthrough pressure is a function of the free distance between the assembled spheres. In the calculated function of the breakthrough pressure against the particle–particle distance, p^* approximates a value of 9.5 at zero distance, with a contact angle of mercury of 140°.

The two-step intrusion curve results in a bimodal pore size distribution when the Washburn equation is applied. This is exemplified by Fig. 2, showing the cumulative and relative pore size distribution of aggregates, made of batch B241/IV by gravity settling.

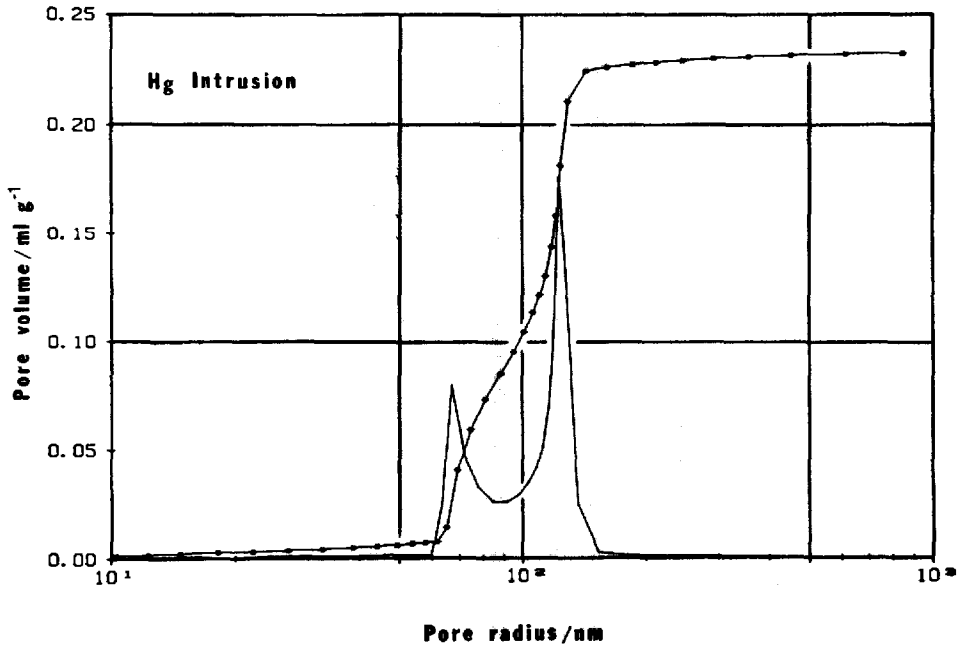

Fig. 2. Cumulative pore size distribution curve of batch B241/IV (d_p = 1002 ± 21.2 nm), obtained by mercury porosimetry (intrusion branch, surface tension of mercury = 480 mN/m, contact angle of mercury = 140°C).

The highly ordered structure of aggregates made by settling was evidenced by the SEM images (see Fig. 3b). There are domains with a close-packed structure within the layers and a vertical stacking of spheres in the layers above and below. This structure is identical to that postulated by Mayer and Stowe[32,33] in their model. The ordered domains are interrupted by defects. A preferred formation of densest horizontal layers and a more open structure between the layers was also observed in the flocculation of silica sols in the presence of detergents. According to Iler[37], the aggregates "grow as sheetlike layers and attach themselves to the growing sheet only around the edges of the sheet, where ionic repulsion is least". The preferred attachment of spheres at the edges of aggregates was also confirmed by potential-energy calculations[38]. Luck *et al.*[39] examined the structure of packed spheres of styrene lattices of 0.8 μm diameter. Their experiments and calculations showed that the cubic structure is energetically slightly preferred over the hexagonal. Similar observations were made for the samples described in this paper. In contrast to the aggregates made by settling, the arrays of silica beads obtained by the slurry technique looked highly disordered and displayed a much more open structure (Fig. 3a).

A more reliable structure analysis was performed by applying stereo-SEM to the aggregates. Images and photographs were taken from a series of different angles to assess the position of the beads in the x,y and z coordinates of the structure. A typical result is shown in Fig. 4. This approach allowed us to compute the sequence of layers as well as the layer-by-layer distance. Again, the close-packed structure was confirmed in the horizontal layers.

In conclusion, the detailed diagnosis of the aggregates has shown that gravity settling provides the densest structure within and between the layers and also less defects between the ordered domains than other techniques. The latter seem to be responsible for not approaching the theoretical porosity of 26% of a close-packed assemblage of spheres. By employing submicron silica beads it was further evidenced that long *n*-alkyl silanes, bonded to the external surface, inhibit dense packing of aggregates.

Packing procedures and performance of columns packed with 1–2-μm non-porous monodisperse C_{18}-bonded silicas

For application in reversed-phase HPLC, the calcined and rehydroxylated silica beads were subjected to silanization by reaction with *n*-octadecyldimethylchlorosilane according to a procedure described elsewhere[12]. As the carbon content of the C_{18}-bonded phase was about 0.2% (w/w) and hence in the range of the reproducibility of the carbon elemental analysis (which is *ca.* $\pm$0.2%), the ligand density could not be calculated from the carbon content. An indirect means is to compare the capacity factors of solutes on the non-porous C_{18}-bonded phase with those on a porous C_{18}-bonded silica of known surface area and ligand density under constant eluent conditions, taking into account the differences in the specific surface areas between the two phases. A direct method of assessing the ligand density is to employ a ^{14}C-enriched silane in the surface reaction and to derive the carbon content of the bonded phase by means of scintillation measurements. Nonetheless, comparison of the retention data showed no difference in the selectivity of the non-porous and porous C_{18}-bonded silicas when the same surface modification procedure and identical chromatographic conditions were used. In order to achieve the same capacity factors with the

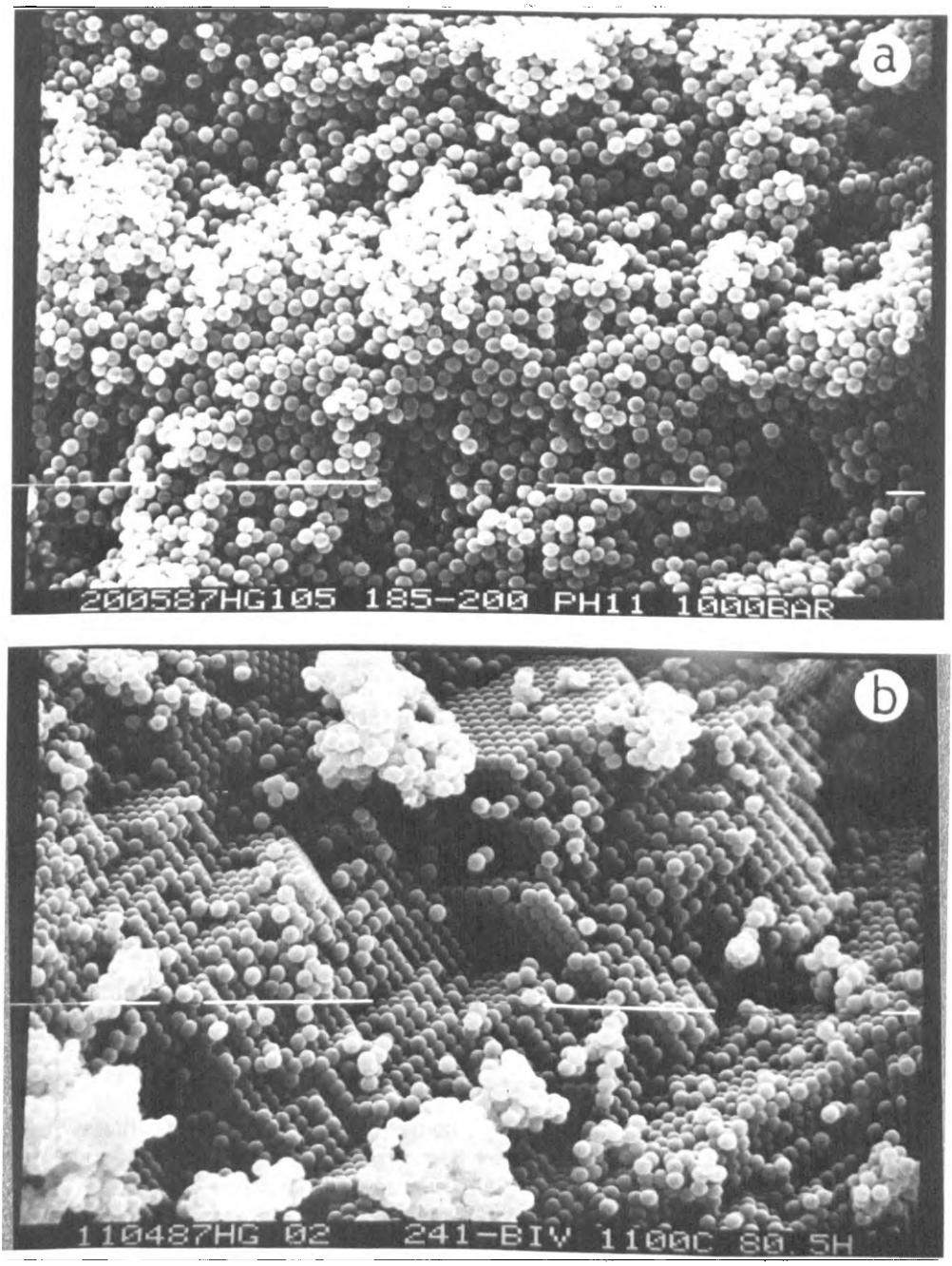

Fig. 3. Scanning electron micrographs of compacted spheres, obtained by (a) the slurry technique and (b) centrifugation. (Batch B241/IV). Bar = 10 μm.

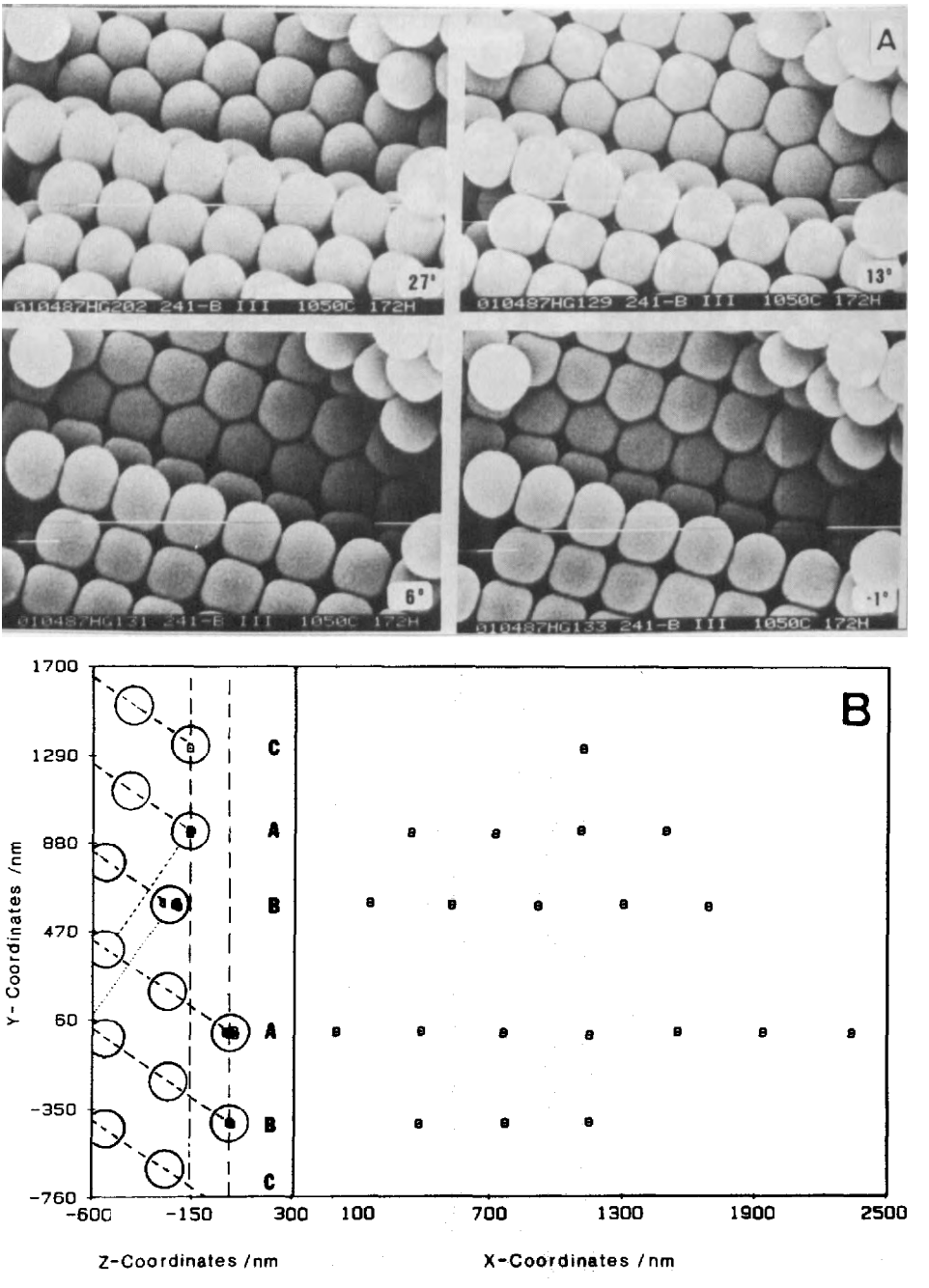

Fig 4. (A) Stereo scanning electron micrograph of aggregates spheres (batch B241/III, $d_p = 431 \pm 9.2$ nm). (B) Assessment of the position of beads in the x,y,z coordinates in the structure.

non-porous C_{18}-bonded silica as with the porous C_{18}-bonded silica, *e.g.*, Hypersil ODS (Shandon, U.K.), the water content of the water–acetonitrile eluent must be increased to 80% (v/v) compared to 40% (v/v) with the Hypersil column.

Although in the aggregation experiments the soft techniques, like gravity settling and centrifugation, gave superior packing structures and higher packing densities than the hard techniques, the slurry technique applied at constant flow-rate and moderate pressures up to 50 Pa and gravity settling in an ethanol–water suspension resulted in nearly the same performance characteristics. In time experience showed that the absence of dead volumes at the column ends was of decisive importance for the column performance. Best results were obtained with Hyperchrom columns (Bischoff) and endfittings made of paper filters, supported by metal frits. The total porosity of the fittings was less than 0.2 μm.

In order to utilize the performance of the 1–2-μm particle columns fully, the HPLC equipment has to meet a number of specifications and requirements which were treated in depth by Guiochon[40].

The use of short columns, *ca.* 50 mm long, first limits the maximum value of the sample volume $V_{S,M}$

$$V_{S,M} = \lambda \Theta \pi \frac{d_c^2}{4} \varepsilon_t (1 + k') (L H)^{\frac{1}{2}} \quad (6)$$

where λ is a numerical factor, reflecting the shape of the injection profile, Θ a factor characterizing the relative increase of the zone width, d_c the column inner diameter, ε_t the total porosity of the column and k' the solute capacity factor. Setting $\lambda = 2$, $\Theta = 0.1$, $d_c = 4.6$ mm, $\varepsilon_t = 0.35$, $k' = 0$, $L = 53$ mm and $H = 6$ μm, $V_{S,M}$ is calculated to be 0.65 μl. The value corresponds to the volume of the sample loop of the Rheodyne injection system employed.

The sample mass to be injected is equal to the product of the sample volume and the sample concentration. On account of the difference in the surface of stationary phase between the porous and the non-porous C_{18}-bonded silicas of about 50, the applicable sample concentration is correspondingly reduced. Column mass loadability for low-molecular-weight compounds thus decreases from about 1 mg per g of porous reversed-phase packing to about 20 μg for the non-porous packing.

When 1–2-μm particles are used, the column back pressure, ΔP, is a limiting factor with regard to the column length. ΔP is given by

$$\Delta P = u \eta L \Phi / d_p^2 \quad (7)$$

where u is the linear velocity of the eluent, η the eluent viscosity, and Φ the column resistance factor. Setting $u = 5$ mm/s, $\eta = 1$ mNs/m^2, $L = 53$ mm, $\Phi = 620$ ($\varepsilon_t = 0.35$), and $d_p = 2.1$ μm, a column back-pressure of 37.3 MPa results. A pressure drop of 37.3 MPa = 373 bar corresponds to a volume flow-rate of 1.74 ml/min. Plots of the column back-pressure against the flow-rate, f_v, were measured for a column of 53 × 4.6 mm, packed with 2.1-μm particles upwards and downwards in several cycles, and gave a straight line with values exactly as predicted by eqn. 7. The equipment used in this study allowed a maximum pressure of about 60 MPa.

On columns packed with 1–2-μm particles, operated at high flow-rates, frictional

heat effects become noticeable. They lead to an additional band broadening[41]. As a rule-of-thumb, the temperature difference, ΔT, between the column head and column exit is related to d_c and d_p as[42]

$$\Delta T = \Psi (d_c^2 \; v \; / \; d_p^4) \tag{8}$$

where Ψ is a constant and v the reduced linear velocity of the eluent. Eqn. 8 shows that ΔT increases by a factor of 30 in going from a 5- to a 2-μm particle column under otherwise constant conditions (column dimensions, eluent composition).

To keep the contribution of the volume of the connecting tubes to the column performance to a minimum, capillaries of 0.1 mm I.D. and 50 mm total length were employed.

The cell volume and the response time of the detector are critical parameters in the operation of short 1–2-μm particle columns. According to Guiochon[40], the maximum allowable cell volume is calculated to be

$$V_{d,M} = \Theta \frac{\pi \; d_c^2}{4} (1 + k') \; h \; d_p \; N^{\frac{1}{2}} \tag{9}$$

where h is the reduced plate height and N the plate number of the column. Setting $\Theta = 0.1$, $d_c = 4.6$ mm, $\varepsilon_t = 0{,}35$, $k' = 0$, $h = 3$, $d_p = 2.1$ μm and $N = 8800$, $V_{d,M}$ is calculated to be 0.3 μl. The cell volume of the UV detector employed in this study was

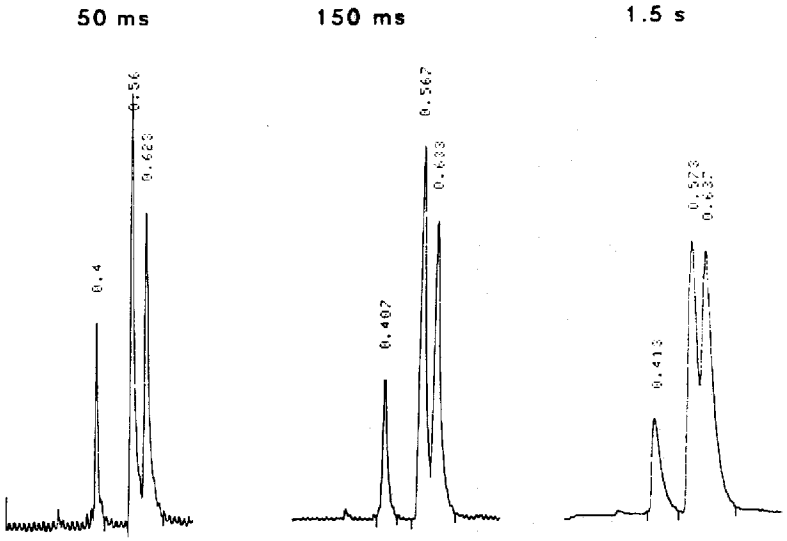

Fig. 5. Effect of the time constant, τ, of the UV detector on the chromatographic resolution. Conditions: column, 53 mm × 4.6 mm I.D. Monospher RP-18, d_p = 2.1 μm; eluent, water–acetonitrile (60:40, v/v); flow-rate, 1.25 ml/min; detection, UV at 254 nm, τ = 50 ms, 150 ms or 1.5 s. Sequence of analytes: naphthalene, biphenyl, fluorene. The numbers at the peaks represent retention times in min.

0.6 μl. The maximum permissible time constant, τ_M required to avoid a noticeable loss in column efficiency is given by

$$\tau_M = \Theta \, t_R / N^{\frac{1}{2}} \tag{10}$$

Setting $\Theta = 0.1$, $N = 8800$ and $t_R = 10\,(60)$ s, τ_M is calculated to be 10 (60) ms. No UV detectors are commercially available with time constants smaller than 50 ms. Fig. 5 demonstrates the influence of the time constant at $\tau = 5$ ms, 150 ms and 1.5 s on the chromatographic resolution of a three-compound mixture on a 53 × 4.6 mm column, packed with 2.1-μm non-porous C_{18}-bonded silicas.

Predicted and actual column performance

Inspection of the plots of h against v indicates optimum values at $h \approx 3$ and $v \approx 5$ (ref. 43). The reduced linear velocity is given by

$$v = \frac{u \, d_p}{D_{im}} = 5 \tag{11}$$

where D_{im} is the solute diffusion coefficient in the eluent.

Setting $D_{im} = 2 \cdot 10^{-9}$ m^2/s for a low-molecular-weight compound in a water–acetonitrile (60:40, v/v) eluent and $d_p = 2.1$ μm, gives $u = 5$ mm/s. The reduced plate height of $h = 3$ generates a plate height of $H = 3\,d_p = 6$ μm for particles of $d_p = 2.1$ μm or a plate number of 8800 at a column length of 53 mm.

Fig. 6 shows a plate height *versus* linear velocity plot, obtained with a 53 mm × 4.6 mm column, packed with non-porous 2.1-μm C_{18}-bonded silica beads. The plate height values between $2 < u < 5$ mm/s are scattered in the range from 5 to 8 μm and reflect the excellent performance of the columns. It is further evident that the plate height at a constant u value increases with decreasing solute capacity factor. This is a clear indication that extra-column contributions to the plate height are present and, hence, affect the peak width of the early-eluted compounds more than that of the late-eluted compounds.

Due to extra-column contributions to the plate height and due to the fact that H was determined by the tangent method, the parameters A, B and C of the Knox equation cannot be reliably estimated by fitting the experimental H *versus* u curves in Fig. 6.

CONCLUSION

As shown in the aggregation experiments of non-porous 1-μm silica beads by centrifugation, gravity settling and the slurry technique, stable suspensions of about pH 10 are required to achieve a high packing density. The dry-bag isostatic compression technique gave dense aggregates only when pressures in excess of 300 MPa were applied. Silica beads with bonded ethylsilyl groups aggregated by gravity settling resulted in denser bodies than those with bonded *n*-octylsilyl groups and even untreated silica. Of all techniques employed, gravity settling gave aggregates with the densest and most highly ordered structure; *i.e.*, a close-packed structure in the horizontal layers and a vertical stacking in between the layers. This was evidenced by

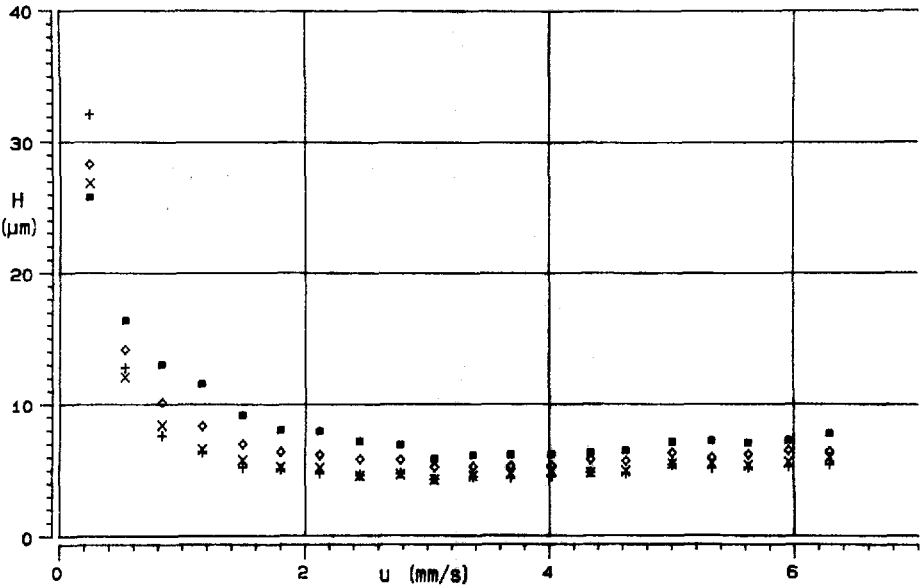

Fig. 6. Plot of the theoretical plate height, H, against the linear velocity of the eluent, u. Conditions: column, 53 mm × 4.6 mm I.D. Monospher RP-18, d_p = 2.1 µm; eluent, water–acetonitrile (60:40, v/v); detection, UV at 254 nm, flow-cell volume 0.6 µl, τ = 50 ms; injection volume, 0.5 µl. Solutes: ■ = naphthalene (k' = 0.39); ◇ = anthracene (k' = 1.18); × = pyrene (k' = 1.74); + = chrysene (k' = 2.99).

stereo-SEM images. The high breakthrough pressure p^* of 8–10 obtained by mercury intrusion on these aggregates served as an additional indication. In contrast, the aggregates made by the slurry technique displayed a more open, random-type structure.

Batches of *n*-octadecyl-modified non-porous 1–2-µm silicas were employed for chromatographic studies. Columns of 53 mm × 4.6 mm I.D. were packed by gravity settling and by the slurry technique (constant flow-rate, end pressure 60 MPa). The columns packed by the two techniques gave nearly the same performance characteristics in terms of pressure–flow-rate and plate height–linear velocity dependence. The generation of less dense column beds by gravity settling compared to the previously described aggregates is probably attributed to the fact that the extent of free settling when the particles sediment in a column is somewhat reduced. As a consequence, all columns used were slurry-packed. In order to use the short columns for fast separations of less than 1 min, the injection volume must be about 0.6 µl, the volume of the UV detector cell about 0.3 µl and the time constant of the detector < 50 ms. In addition, dead volume contributions must be avoided. Even then the peak dispersion (plate height) of the early-eluted peaks was found somewhat lower than those of the late-eluting peaks, indicating the presence of extra-column effects. This might be caused by the type of injection system employed which did not permit a fast injection.

In general, the plate height–linear velocity plots showed the expected performance characteristics for micron-size packings: a plate height value corresponding to two to five times the mean particle diameter and at a linear velocity of $u \gg 3$ mm/s

with nearly no loss in column efficiency up to 6.0 mm/s. At about 6.4 mm/s corresponding to a flow-rate of 2.2 ml/min the pressure limit of the HPLC equipment was reached.

REFERENCES

1 L. R. Snyder and J. J. Kirkland, *Introduction to Modern Liquid Chromatography*, Wiley, New York, 1979, pp. 202–218.
2 G. Guiochon and A. Katti, *Chromatographia*, 24 (1987) 165–189.
3 M. Verzele, J. van Dijck, P. Musche and C. Dewaele, *J. Liq. Chromatogr.*, 5 (1982) 1431–1448.
4 C. Dewaele and M. Verzele, *J. Chromatogr.*, 260 (1983) 13–21.
5 M. Verzele, C. Dewaele and D. Duquet, *J. Chromatogr.*, 391 (1987) 111–118.
6 K. K. Unger, H. Giesche and J. N. Kinkel, *Ger. Pat.*, DE-3534 143.2 (1985).
7 C. Dewaele and M. Verzele, *J. Chromatogr.*, 282 (1983) 341–350.
8 K. K. Unger, G. Jilge, B. Eray and I. Novak, paper presented at the *10th International Symposium on Column Liquid Chromatography, San Francisco, CA, May 18–23, 1986*, paper 502.
9 N. D. Danielson and J. J. Kirkland, paper presented at the *10th International Symposium on Column Liquid Chromatography, San Francisco, CA, May 18–23, 1986*, paper 503.
10 N. D. Danielson and J. J. Kirkland, *Anal. Chem.*, 59 (1987) 2501–2506.
11 W. Stöber, A. Fink and E. Bohn, *J. Colloid Interface Sci.*, 26 (1968) 62.
12 K. D. Lork, K. K. Unger and J. N. Kinkel, *J. Chromatogr.*, 352 (1986) 199–211.
13 K. K. Unger, E. Schadow and H. Fischer, *Z. Phys. Chem. (N.F.)*, 99 (1976) 245–256.
14 S. J. Gregg and K. S. W. Sing, *Adsorption, Surface Area and Porosity*, Academic Press, London, 1982.
15 E. Schadow and K. K. Unger, *High Temp.–High Pressures*, 9 (1977) 591–594.
16 R. K. Iler, in E. Matijevič (Editor), *Surface and Colloid Science*, Vol. 6,Wiley, New York, 1973, pp. 39–65.
17 G. D. Parfitt and K. S. W. Sing, *Characterization of Powder Surfaces*, Academic Press, London, 1976, p. 10.
18 H.Rumpf, *Chem.–Ing.–Tech.*, 46 (1974) 1–11.
19 H.Schubert, *Chem.–Ing.–Tech.*, 51 (1979) 266–277.
20 H. Heesch and F. Laves, *Z. Kristallogr.*, 85 (1933) 443.
21 E. Manegold, *Kapillarsysteme*, Vol. 1, Strassenbau, Chemie & Technik Verlag, Heidelberg, 1955.
22 D. G. Kadaner, V. M. Lukjanovich and L. V. Radushkevich, *Dokl. Akad. Nauk SSSR*, 87 (1952) 1001.
23 H. P. Meissner, A. S. Michaels and R. Kaiser, *Ind. Eng. Chem. Prod. Res. Dev.*, 3 (1964) 202.
24 K. Ridgway and K. J. Tarbuck, *Br. Chem. Eng.*, 12 (1967) 385.
25 A. P. Karnaukhov, in S. Modry and M. Svata (Editors), *Pore Structure and Properties of Materials, Proc. RILEM/IUPAC Conf., Prague, 1973; Preliminary Report*, Part I, Academia, Prague, pp. A3–A33.
26 S. Buckowiecki, B. Straube and K. K. Unger, in J. M. Haynes and P. Rossi-Doria (Editors), *Principles and Applications of Pore Structural Characterization*, Arrowsmith, Bristol, 1985, pp. 43–55.
27 R. G. Avery and J. D. F. Ramsay, *J. Colloid Interface Sci.*, 42 (1973) 597.
28 A. P. Karnaukhov, *Kinet. Katal.*, 12 (1971) 1025.
29 A. P. Karnaukhov, *Kinet. Katal.*, 12 (1971) 1235.
30 J. Rouqerol, personal communication.
31 L. K. Frevel and L. J. Kressley, *Anal. Chem.*, 35 (1963) 1492.
32 R. P. Mayer and R. A. Stowe, *J. Colloid Sci.*, 20 (1965) 893.
33 R. P. Mayer and R. A. Stowe, *J. Phys. Chem.*, 70 (1966) 3867.
34 S. Kruyer, *Trans. Faraday Soc.*, 54 (1958) 1758.
35 D. M. Smith and D. L. Stermer, *J. Colloid Interface Sci.*, 111 (1985) 160.
36 R. P. Iczkowski, *Ind. Eng. Chem.*, 5 (1966) 516; 6 (1967) 263.
37 R. K. Iler, in E. Matijevič (Editor), *Surface and Colloid Science*, Vol. 6, Wiley, New York, 1973, pp. 58–60.
38 I. L. Thomas and K. H. McCorkle, *J. Colloid Interface Sci.*, 36 (1971) 110.
39 W. Luck, M. Klier and H. Wesslau, *Naturwissenschaften*, (1963) 37.
40 G. Guiochon, in Cs. Horváth (Editor), *HPLC —Advances and Perspectives*, Vol. 2, Academic Press, New York, 1980, pp. 1–54.
41 H. Poppe and J. C. Kraak, *J. Chromatogr.*, 282 (1983) 399–412.
42 S. J. Van der Waal, *LC, Mag. Liq. Chromatogr. HPLC*, 3 (1985) 488–496.
43 J. H. Knox and H. P. Scott, *J. Chromatogr.*, 282 (1983) 297–313.